The Superatom States of Fullerenes and Their Hybridization into the Nearly Free Electron Bands of Fullerites

Jin Zhao,[†] Min Feng,[†] Jinlong Yang,[§] and Hrvoje Petek[†,‡,*]

[†]Department of Physics and Astronomy, and Petersen Institute of NanoScience and Engineering, University of Pittsburgh, Pittsburgh, Pennsylvania 15260, [‡]Donostia International Physics Center, P. Manuel de Lardizabal 4, 20018 San Sebastian, Spain, and [§]Hefei National Laboratory for Physical Sciences at Microscale, University of Science and Technology of China, Hefei, Anhui, China

ABSTRACT Motivated by the discovery of the superatom states of C_{60} molecules, we investigate the factors that influence their energy and wave function hybridization into nearly free electron bands in molecular solids. As the $n = 3$ solutions of the radial Schrödinger equation of the central attractive potential consisting of the short-range C atom core and the long-range collective screening potentials, respectively, located on the icosahedral C_{60} molecule shell and within its hollow core, superatom states are distinguished by their atom-like orbitals corresponding to different orbital angular momentum states ($l = 0, 1, 2,...$). Because they are less tightly bound than the π orbitals, that is, the $n = 2$ states, which are often exploited in the intermolecular electron transport in aromatic organic molecule semiconductors, superatom orbitals hybridize more extensively among aggregated molecules to form bands with nearly free electron dispersion. The prospect of exploiting the strong intermolecular coupling to achieve metal-like conduction in applications such as molecular electronics may be attained by lowering the energy of superatom states from 3.5 eV for single chemisorbed C_{60} molecules to below the Fermi level; therefore, we study how the superatom state energies depend on factors such as their aggregation into 1D−3D solids, cage size, and exo- and endohedral doping by metal atoms. We find, indeed, that if the ionization potential of endohedral atom, such as copper, is sufficiently large, superatom states can form the conduction band in the middle of the gap between the HOMO and LUMO of the parent C_{60} molecule. Through a plane-wave density functional theory study, we provide insights for a new paradigm for intermolecular electronic interaction beyond the conventional one among the sp^n hybridized orbitals of the organic molecular solids that could lead to design of novel molecular materials and quantum structures with extraordinary optical and electronic properties.

KEYWORDS: C_{60} · superatom states · molecular metal · endohedral doping

C_{60}, the most stable fullerene, is an atom-like building block of fullerite solids with potential applications in molecular electronics and optoelectronics.[1−4] By doping with alkali atoms, C_{60} fullerites can be transformed from semiconducting into the metallic, insulating, superconducting, and magnetic phases depending on the concentration and the composition of the dopant atoms.[5−8] Monolayer C_{60} films on metal surfaces become conductive normal to the molecular plane through charge transfer from the substrate to the lowest unoccupied molecular orbital (LUMO). Within a chemisorbed C_{60} molecular monolayer, however, the electron delocalization, as probed by the scanning tunneling microscopy (STM) and spectroscopy, is constrained by the poor intermolecular wave function overlap between the highly degenerate and tightly bound σ and π orbitals of the proximate molecules.[9−15]

Nevertheless, nearly free electron (NFE)-like behavior has been observed for the unoccupied states of C_{60} aggregates on metal surfaces in angle-resolved two-photon photoemission (2PP) and low-temperature scanning tunneling microscopy (LT-STM) experiments.[16,17] In the LT-STM experiments, we discovered a series of atom-like molecular orbitals, which are distinct from the well-known σ and π orbitals that form through hybridization of the atomic s and p orbitals on C atom nuclei. On the basis of the experimental and theoretical spatial distributions of these orbitals, we dubbed them the superatom molecular orbitals (SAMOs).[17] Instead of being bound to individual C atoms and deriving their shapes through hybridization between the atomic centers like the σ and π orbitals, SAMOs assume the radial and angular distributions of spherical harmonic functions that are defined by the central potential of the hollow C_{60} molecular core. The SAMO wave functions extend well beyond the more tightly bound π orbitals, which allows them—when C_{60} molecules are brought to approximately their van der Waals distance of ~1.0 nm[18]—to hybridize akin to the s, p, and d orbitals of atoms. Remarkably, for molecular materials, when C_{60} molecules are arranged into 1D, 2D, or 3D structures, according to the 2PP and LT-STM measurements, SAMOs hybridize into s-electron metal-like NFE bands.[16,17]

The atom-like self-organization of C_{60} molecules into higher dimensional aggregates and the metal-like NFE band

*Address correspondence to petek@pitt.edu.

Received for review December 4, 2008 and accepted March 26, 2009.

Published online April 7, 2009.
10.1021/nn800834k CCC: $40.75

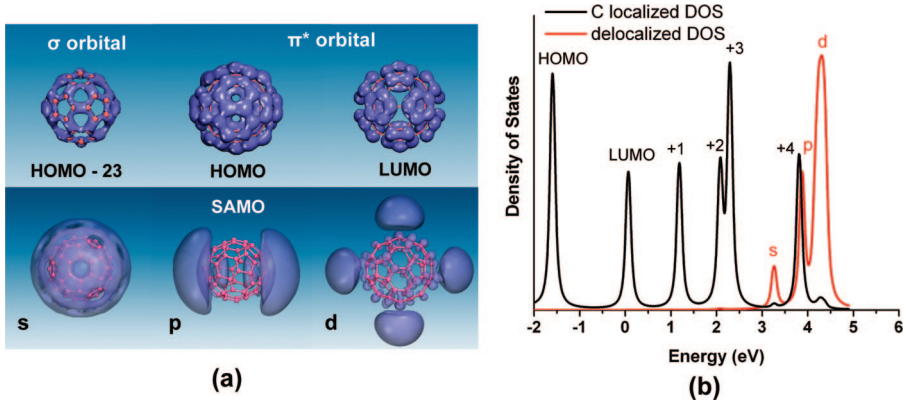

Figure 1. (a) DFT calculated orbitals of the σ (HOMO and LUMO) and s-, p-, and d-SAMO states. (b) Density of states of a single C_{60} molecule is separated into contributions that are derived from orbitals localized on individual C atoms (black line) and those that are not bound to C atoms (red line). The energy of LUMO is set to zero.

formation derived from hybridization of SAMOs could enable novel applications in molecular electronics.[19,20] For instance, 1D and 2D aggregates of C_{60} molecules could be exploited as quantum wires and quantum wells with single-molecule-wide dimensions.[16,17,20] For an isolated C_{60} molecule, however, the lowest energy s-SAMO with the orbital angular momentum $l = 0$ is 3.28 eV above the LUMO.[17,21−23] Positioned above the unoccupied LUMO to LUMO+3 π* orbitals, the s-SAMO can decay by the internal conversion on the femtosecond time scale, precluding its role in charge transport.[16] Therefore, to achieve practical SAMO-mediated electron transport, it is essential to tune their energy closer to the Fermi level (E_F). That this should be possible is evident from intercalated graphite, for which the interstitial metal atoms stabilize the related interlayer states to below E_F,[24,25] as well as from the superatom NFE character of the conduction band minima of hexagonal BN and BN nanotubes.[26] With this goal in mind, we study how the fullerene packing, cage size, and exo- and endohedral doping with metal atoms affect the energy momentum dispersion of SAMO-derived NFE bands of 1D, 2D, and 3D fullerite aggregates.

RESULTS AND DISCUSSION

SAMOs of an Isolated C_{60} Molecule. The electronic structure of C_{60} molecules has been studied extensively by a broad range of experimental and theoretical methods.[27−35] The highly degenerate valence states of this icosahedral symmetry molecule consist of the deeply bound σ orbitals and above them the π orbitals.[35] Several of the π* orbitals, especially the HOMO, LUMO, LUMO+1, and LUMO+2[17,36] have been resolved at the molecular orbital level by LT-STM.[13,23,27,37,38] The LT-STM images can be interpreted in terms of the local density of states (LDOS) of the π antibonding orbitals on the C atom pentagons or hexagons, which mediate the tunneling through C_{60} molecules.[38]

Our recent STM spectroscopic study focused on the unoccupied electronic structure of C_{60} molecules on copper surfaces in the 2.8−5.2 V range, which is higher than has been previously studied.[17] By means of z-V spectroscopy, we could study several new unoccupied states that exist above 3.5 V.[17,39] d*I*/d*V* spectroscopic imaging in the 2.8−3.2 eV range revealed that the LUMO+2 state retains the π* molecular orbital character. LUMO+2 and LUMO+3 are difficult to resolve and distinguish through d*I*/d*V* imaging or z-V spectroscopy because they are nearly degenerate and have similar LDOS distributions. Above 3.5 V, the π* molecular orbital LDOS in the d*I*/d*V* images of single C_{60} molecules is supplanted by orbitals with more simple, diffuse character; when C_{60} molecules self-assemble into 1D chains and 2D islands,[17,20] single molecule contrast vanishes from the d*I*/d*V* images, indicating that the diffuse orbitals hybridize into delocalized bands. We performed plane-wave DFT calculations on isolated C_{60} molecules and projected out the atom-localized DOS to identify the remaining diffuse molecular orbitals as the SAMOs. As shown in Figure 1a, these diffuse orbitals are centered on the hollow core rather than being bound to the individual carbon atoms on the C_{60} molecule shell. Because they resemble the spherical harmonic functions corresponding to the orbital angular momentum states with $l = 0$, 1, and 2, we label SAMOs with the s, p, and d notation of atomic orbitals. In agreement with the experiments, the lowest energy s-SAMO is predicted above the LUMO+3 state (Figure 1b). Although it is predicted at ~3.8 eV, LUMO+4 has not been observed by LT-STM, most likely because the STM imaging is more sensitive to the more diffuse SAMO states at nearly the same energy.

In order to establish the physical origin of SAMOs, in Figure 2, we plot the angle-averaged radial potential of the C_{60} molecule and wave functions obtained by solving the Schrödinger equation for this potential. The radial potential in Figure 2a is composed of a deep well at the C atom shell and a shallow, nearly constant attractive well within the center of the hollow core. The wave functions obtained for this radial potential qualitatively reproduce the angularly averaged DFT probability densities of the σ, π, and SAMO states in Figure 2b. Solutions of the Schrödinger equation are defined by their principal quantum number n and the angular momentum quantum number l. The σ and π orbitals, respectively, with 0 and 1 radial nodes, correspond to the $n = 1$ and 2 solutions. The SAMO wave functions have two radial nodes that approximately coincide with the π orbital density maxima and, therefore, correspond to the $n = 3$ states. By performing the calculations with different relative depths for the core and the

shell potentials, we found that the $n = 1$ and 2 states are dominantly bound by the shell potential, while the $n = 3$ SAMO wave functions critically depend on the depths of both potentials.

The origin of the attractive core potential can be traced to the screening of an electron charge by the charge density on the C atom shell through the short-range exchange-correlation and long-range Coulomb interactions.[40] For a 2D graphene sheet, the many-body screening gives rise to a double Rydberg series of image potential (IP) states with even and odd symmetry that converge to the vacuum level and have NFE character parallel to the molecular plane.[26,40−42] When a 2D graphene sheet is wrapped to form a spherical C_{60} molecule, the lowest energy IP state with even symmetry correlates with the $n = 3$ s-SAMO state. Consequently, the central potential can be attributed to the short-range exchange and correlation potential; the long-range Coulomb potential, which makes a significant contribution only on the outside of C_{60} molecule and is not included in the DFT calculation, is essential for describing the external potential.[40] The wave functions above the s-SAMO (*i.e.*, $n = 3$, $l > 0$, and $n > 3$) solutions of the radial potential exist mainly on the outside of the C_{60} shell, and therefore, to describe them more accurately would require inclusion of the Coulomb contribution to the radial potential. The binding energy of s-SAMO with respect to the vacuum level is −0.94 eV, compared with −1.17 eV for the DFT calculation for the lowest energy IP state of graphene.[40] The lower binding energy can be attributed to the stronger quantum confinement of the 0D wave function with respect to the 2D one.

The experimentally observed SAMOs are the lowest members of a diffuse series of states that should converge in a Rydberg series to the vacuum level. In fact, the Rydberg character of high angular momentum $n = 3$ states has been observed by Boyle *et al.* for the neutral C_{60} molecule[42] under the molecular beam conditions.[42] We distinguish SAMOs from Rydberg states, however, because the former are contained substantially, and for the s-SAMO, dominantly within the hollow C_{60} core, while the latter see the core as a point charge. Whereas SAMOs are unique to hollow molecules, any molecule or molecular anion will have Rydberg states.

Hybridization of SAMOs in C_{60} Assemblies. Because SAMOs are more diffuse than the σ and π orbitals, their hybridization within C_{60} molecular aggregates should give rise to delocalized bands with larger bandwidths and therefore greater energy stabilization than the intermolecular hybridization among the atomic sp^n orbitals. Therefore, we studied theoretically how SAMOs hybridize when C_{60} molecules are assembled into 1D wires, 2D quantum wells, and 3D solids. As already noted, the vanishing of molecular contrast in d*I*/d*V* images of 1D and 2D assemblies is indicative of extensive wave function delocalization.[17] We calculated the electronic structure of an infinite, one C_{60} molecule wide chain for intermolecular separations *a* ranging from 0.9 to 1.8 nm. For the 2D and 3D close packed structures, we set the distance between the nearest neighbor C_{60} molecules to their van der Waals diameter of 1.0 nm.[18,43] For comparison, the intermolecular distances in the 1D and 2D quantum structures on Cu(110) and Cu(111) surfaces, respectively, are 1.07 and 1.02 nm.[17,20] The 1D−3D band structures were calculated, and the effective masses m^* were obtained from the curvatures of the bands at their respective Γ points. The effective masses m^* are reported in Table 1 as multiples of the free-electron

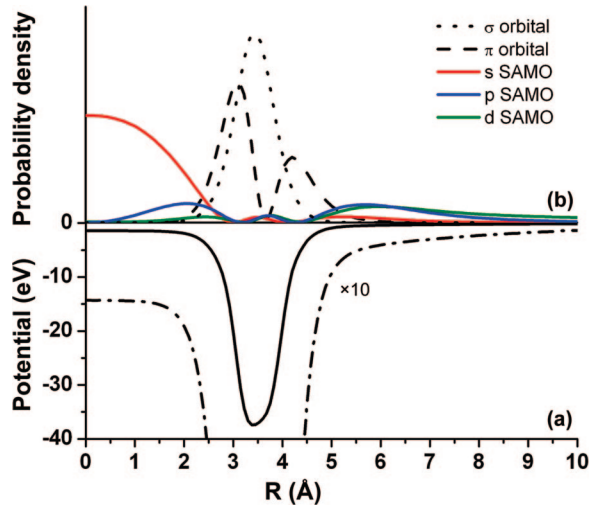

Figure 2. Calculated angle-averaged radial potential and wave functions of single C_{60} molecules. The dashed line in (a) is the potential magnified 10 times.

TABLE 1. Effective Masses of the Energy Bands for the 1D, 2D, and 3D C_{60} Supramolecular Assemblies

	a (nm)	LUMO	s-SAMO	p_y, p_z-SAMO	p_x-SAMO
1D structure	0.9	0.25−1.5	1.0	1.0	−0.3
	1.0	3.0−7.0	1.0	1.1	−0.2
	1.1	4.0−10.0	1.4	1.4	−0.3
	1.2	14.0−20.0	1.6	1.6	−0.4
	1.3	30.0−60.0	2.7	2.8	−0.5
	1.4	100.0−580.0	3.9	4.0	−0.6
	1.5	∼∞	4.4	4.5	−0.8
	1.8		12.0	12.5	−2.0

		LUMO	s-SAMO	p_x-SAMO[a]	p_y-SAMO[a]	p_z-SAMO
2D structure	C_{60}	3.0−6.5	1.0	−0.1	−0.3	1.0
	Li_2C_{60}	1.5−2.1	1.0	−0.5	−0.7	2.1
	Li@C_{60}b	2.0−5.0	2.0	−0.7	−1.6	1.8
	Li@C_{60}c	1.5−5.5	1.5	−0.5	−0.5	1.2
	Ca@C_{60}b	2.0−7.0	1.6	−0.6	−1.4	1.0
	Cu@C_{60}	2.5−5.0	2.8	−0.5	−0.6	0.8
	C_{60}/Cu(111)	1.5−2.2	1.0	−0.1	−0.3	0.9

		LUMO	s-SAMO	p_z-SAMO
3D structure	C_{60}	3.0−6.5	0.9	−0.3

[a]The p_x and p_y are nearly equivalent because of the icosahedral symmetry of C_{60} molecules. [b]Doping atom at the center of C_{60} molecule. [c]Doping atom at the optimized position.

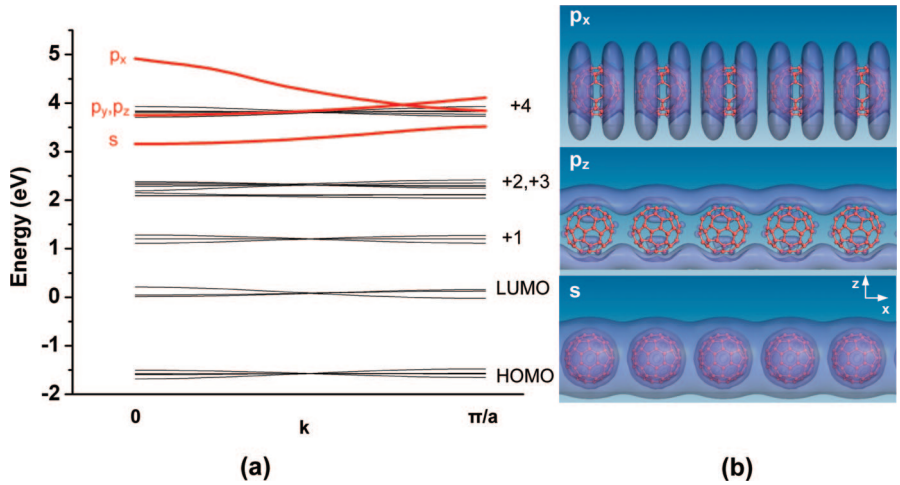

Figure 3. (a) Band structure of a 1D C_{60} quantum wire for $a = 1.0$ nm. The red lines show the energy bands formed by the SAMOs. (b) Orbital distributions of the s-, p_z-, and p_x-SAMOs at $k = 0$ (the Γ point).

mass m_e. The SAMO-derived bands can immediately be distinguished in Figures 3−5 from the LUMO+n-derived bands by their larger band dispersions and, therefore, smaller effective masses. The effective masses obtained for C_{60} molecular assemblies with $a = 1.0$ nm confirm that the bands derived by hybridization of SAMOs will have NFE properties expected for s-electron metals.

In order to further parametrize the NFE bands, we cast the SAMO hybridization within the tight-binding approximation, where we consider only the interaction between the nearest neighbor molecules.[44] The tight-binding band structure can be expressed as

$$E(k) = \varepsilon_0 - \sum_{R=nn} \beta(R) \cdot e^{-ik \cdot R} \qquad (1)$$

where ε_0 is the energy of the band center and $\beta(R) = \langle \phi_0 | h | \phi_{nn} \rangle$ is the hopping integral connecting the nearest neighbors. The hopping integral β in Table 2 is obtained by fitting the SAMO bands to eq 1. The magnitude of β determines the strength of the intermolecular interaction and, therefore, the bandwidth: the larger the overlap, the stronger the dispersion and the broader the width. For the 1D, 2D, and 3D structures, the tight-binding bandwidths correspond to 4β, 9β, and 12β, respectively.

Because our calculations do not include the substrate for the 1D and 2D aggregates, we also performed electronic structure calculations for a 2D monolayer of C_{60} molecules on the Cu(111) surface, such as we investigated experimentally in ref 17. From the close similarity between the SAMO effective masses, hopping integrals, and LUMO−SAMO gaps for the free and supported 2D quantum wells that are reported in Tables 1−3, we conclude that the substrate has a negligible role in conferring the NFE properties to the SAMO-derived bands. Therefore, our conclusions based on the calculations for the free 1D and 2D quantum structures are applicable to a far more practical situation where such structures are supported on solid surfaces.

From our calculations, we conclude that SAMOs hybridize into delocalized bands with NFE dispersion akin to the s and p orbitals of s-electron metals (*e.g.*, alkali atoms). For the simplest example of the 1D C_{60} wire, from the Brillouin zone center to the boundary ($k = 0$ to π/a), the s and p_y/p_z-derived bands disperse to higher energy, whereas the p_x-derived band disperses to lower energy. From the orbital distributions of s- and p-SAMO-derived bands at Γ point in Figure 3b, it is clear that the s- and p_y/p_z-SAMOs hybridize like atomic orbitals into bands with the σ and π bonding character, respectively, whereas the p_x-orbital hybridizes into a band with the σ* antibonding character. We have established that such atom-like hybridization of SAMOs into superatom molecular states occurs by imaging the corresponding σ and π symmetry orbitals of C_{60} molecule dimers.[17]

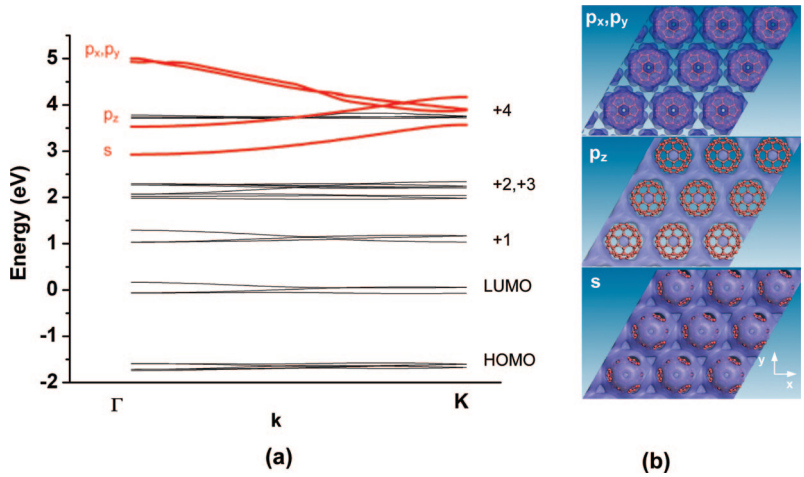

Figure 4. (a) Band structure of a 2D C_{60} quantum well. The red lines show the energy bands formed by the SAMOs. (b) Orbital distribution of the s-, p_x-, p_y-, and p_z-SAMOs at the Γ point.

The diffuse character of SAMOs makes the electronic interaction between the nearest neighbor C_{60} molecules much stronger than when mediated by the σ and π HOMO and LUMO orbitals. From the 1D C_{60} wire calculations, we can see that the onset of significant SAMO hybridization occurs when the distance between C_{60} molecules is ~1.5 nm. Our DFT calculations actually underestimate the interaction strength because the C_{60} potential does not include the long-range Coulomb tail. For

a = 1.5 nm, the s- and p_y/p_z-SAMOs form bands with m^* of about 4.5 times m_e, whereas the interaction between for the p_x orbitals is even stronger corresponding to an effective mass of $0.8m_e$. By contrast, the intermolecular interactions mediated by the triply degenerate LUMO state are negligible. For the van der Waals molecular separation of a = 1.0 nm, m^* of the s-and p_x-SAMO-derived bands decrease to $1.0m_e$ and $0.2m_e$, which is still much smaller than for the LUMO-derived bands. The bandwidth of the 1D s-SAMO band is $4\beta \approx 0.36$ eV, whereas the corresponding bandwidths of the 2D and 3D C_{60} aggregates are even larger at ~0.6 eV. For comparison, the experimental HOMO bandwidths for the prototypical molecular semiconductor pentacene are smaller by a factor of 2 to 3.[15]

The NFE dispersion of SAMO-derived bands is consistent with the previous report of a quantum well state formation for C_{60} overlayers on the Au(111) surface. In an angle and time-resolved 2PP spectroscopic study, Zhu *et al.* reported a state 3.7 eV above E_F with $m^* \leq 1.4m_e$ for the first and second monolayers of C_{60} molecules on the Au(111) surface.[16] They could fit the band dispersions with the tight-binding model using a hopping integral of β = 33 meV. On the basis of a calculated energy level structure from a DFT calculation with an atomic basis set, they attributed this quantum well state to the hybridization of the LUMO+2 or LUMO+3 states. Our calculation with the plane-wave basis sets, which includes the diffuse states, favors the assignment of the 2D C_{60} quantum well state to the s-SAMO-derived band. Compared with the experiment on C_{60}/Au(111) surface, our theoretical calculations predict stronger intermolecular interaction characterized by larger β = 71 meV and smaller m^* of $\sim 1.0m_e$. The weaker experimental interaction can in part be explained by the intermolecular distance of 1.15 nm between C_{60} molecules for the 4×4 superstructure on the Au(111) surface. Because the molecule−surface interaction on the Au(111) surface forces the intermolecule distance to be significantly larger than the van der Waals distance, the larger effective mass is expected; in good agreement with the 2PP experiment, from the 1D calculation, we estimate an effective mass of $\sim 1.5m_e$ for a = 1.15 nm.

Our DFT study shows that the atom-like SAMOs of C_{60} molecules can achieve sufficient wave function overlap for electrons to delocalize over a molecular assembly as would free electrons in an s-electron metal. Therefore, C_{60} molecules may be considered as atom-like building blocks of molecular wires, quantum wells, and molecular crystals, where the hybridization of SAMOs could potentially impart metal-like conductivity.

Motivation for Reducing the LUMO−SAMO Gap. The prospect of exploiting the superatom properties of C_{60} molecules in practical applications has to be tempered by the fact that below SAMOs there exist several LUMO states. The calculated lowest energy s-SAMO is 3.28 eV above the LUMO for an isolated C_{60} molecule. On the basis of the line width analysis of 2PP spectra and the estimated time resolution of their pump−probe measurements, Zhu *et al.* set the lower and upper bounds of 4 and 20 fs for the lifetime of s-SAMO quantum well state.[16] Although it is not known whether the decay occurs by coupling of s-SAMO with the conduction band of Au(111) or by the internal conversion, multiphoton ionization studies of free C_{60} molecules show that the internal conversion from the high-lying electronic states occurs on the <100 fs time scale.[45] The similarity between the z-V spectra of C_{60} molecules on Cu(110) and

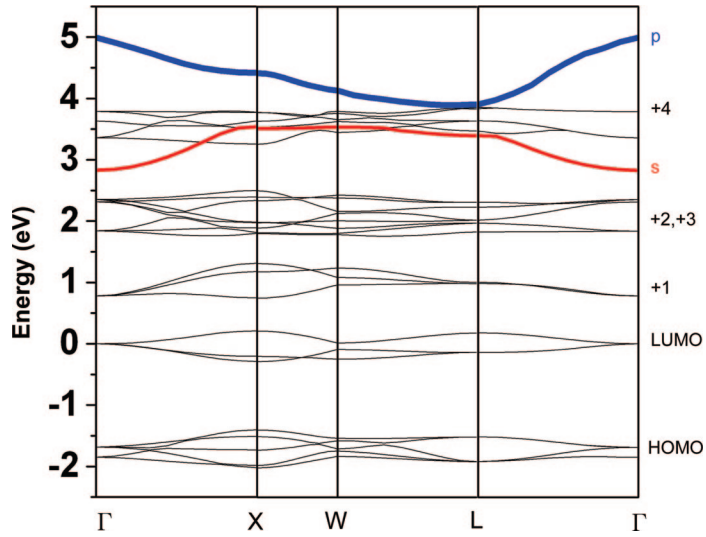

Figure 5. Band structure of a 3D C_{60} crystal. The red line indicates the s-SAMO band. The p-SAMO band is indicated with a thicker blue line because the p_x, p_y, and p_z energy bands are nearly degenerate on account of the icosahedral symmetry of C_{60} molecules.

TABLE 2. Hopping Integral β between SAMOs of the Nearest Neighbor C_{60} Molecules within the Tight-Binding Approximation

		β (meV)		
	a (nm)	s-SAMO	p_y, p_z-SAMO	p_x-SAMO
1D structure	0.9	109	124	−287
	1.0	90	89	−268
	1.1	77	77	−225
	1.2	62	57	−173
	1.3	43	39	−124
	1.4	28	26	−112
	1.5	17	17	−101
	1.8	4	5	−37
		s-SAMO	p_z-SAMO	p_x, p_y-SAMO
2D structure	C_{60}	71	70	−127
	Li_2C_{60}	91	29	−111
	$Li@C_{60}$[a]	20	25	−46
	$Li@C_{60}$[b]	18	19	−91
	$Ca@C_{60}$[a]	21	46	−54
	$Cu@C_{60}$	12	85	−113
	C_{60}/Cu(111)	72	73	−130
		s-SAMO	p-SAMO	
3D structure	C_{60}	53	−83	

[a]Doping atom at the center of C_{60}. [b]Doping atom at the optimized position.

TABLE 3. LUMO−SAMO Gap at Γ Point for the 1D, 2D, and 3D C_{60} Supramolecular Assemblies

		LUMO-SAMO gap at Γ point (eV)		
	a (nm)	s-SAMO	p_y, p_z-SAMO	p_x-SAMO
1D structure	0.9	3.18	3.65	5.23
	1.0	3.16	3.75	4.91
	1.1	3.16	3.70	4.42
	1.2	3.16	3.69	4.23
	1.3	3.20	3.73	4.03
	1.4	3.23	3.76	4.05
	1.5	3.26	3.78	4.05
	1.8	3.28	3.89	3.80
		s-SAMO	p_x, p_y-SAMO	p_z-SAMO
2D structure	C_{60}	2.93	4.95	3.53
	Li_2C_{60}	2.85	4.95	3.47
	Li@C_{60}[a]	1.05	3.37	2.89
	Li@C_{60}[b]	1.90	4.49	3.52
	Ca@C_{60}[a]	0.44	4.11	3.18
	Cu@C_{60}	−0.52	5.22	3.27
	C_{60}/Cu(111)[c]	3.31	5.30	3.90
		s-SAMO	p-SAMO	
3D structure	C_{60}	2.83	5.0	

[a]doping atom at the center of C_{60} [b]doping atom at the optimized position [c]energy is relative to the Fermi level

Cu(111) surfaces suggests that the electronic interactions with the substrate may not be the dominant factor. Because of the anisotropy of the electronic band structure of copper, adsorbates on the Cu(110) surface undergo much faster electronic decay by the resonant charge transfer than for the Cu(111) surface.[46,47] Therefore, if the interaction with the substrate were significantly different, the z-V spectra of C_{60} on Cu(110) would be significantly broader than for the Cu(111) surface. Therefore, for chemisorbed C_{60} molecules on metal surfaces, internal conversion can contribute significantly to the electronic decay of SAMOs. If, however, the SAMO-derived bands could be stabilized to below the LUMO states, or even to the Fermi level, molecular materials with the SAMO-defined charge transport properties might find important applications in molecular electronics.

Strategies for Reducing the LUMO−SAMO Gap. The LUMO−SAMO gap could be reduced by selectively modifying the external and internal potentials that define the SAMO wave functions. Because the tightly bound π orbitals are predominantly defined by the C atom potentials, as well as the hybridization between the nearest neighbor atomic centers, they will be less affected than SAMO wave functions by perturbations that are not on the C atom shell. The perturbations could be in the form of the intermolecular hybridization of SAMOs, which, as noted above, stabilize the corresponding bands. Alternatively, the external perturbations could be through doping with electron-donating materials, such as metal atoms, which can hybridize with the external tails of SAMO wave functions.

Alternatively, tuning the potential of the hollow fullerene core may reduce the LUMO−SAMO gap. Whereas decreasing the fullerene volume increases the depth of its central potential, the concomitant increase in the electron kinetic energy has the opposite effect on the SAMO binding energy with respect to the vacuum level. Thus, there may exist an optimum size and/or shape between the small fullerene limit and graphene that gives the largest binding energy and the smallest LUMO−SAMO gap.

Finally, the internal doping with electron-donating metal atoms could also substantially enhance the central potential. Internal atoms can increase the electron kinetic energy by excluding a part of the internal volume through the Pauli exclusion. They can also enhance the central potential according to the electron binding energy of their ionic core (*i.e.*, the ionization potential). Thus, small s-electron metal atoms with large ionization potentials will stabilize SAMOs most strongly. The degree of mixing between the metal atom and SAMO character will depend, however, on the strength of the potential. Strong mixing will happen for low ionization potential metal atoms because their energies will be the closest to the interacting SAMO energy levels. Because fullerenes have large electron affinities, however, low ionization potential metals will be ionized, and their most stable sites will be in the high charge density regions of the C atom shell off-center from the hollow core. If the ionization potential is sufficiently strong, however, the hybrid orbital between the metal atom and SAMO will be partially occupied, as required for a metal, and the repulsive interaction with the C atom shell will stabilize the metal atom in its center.[48]

SAMO Band Formation. The intermolecular hybridization of SAMOs into 1D−3D bands has a modest effect on decreasing the LUMO−SAMO gap at the Γ point. As can be gleaned from Table 3, the free molecule gap decreases from 3.28 eV for the free molecule to 2.83 eV for the 3D solid. The SAMO energy decrease upon aggregation corresponds approximately to one-half of the bandwidth of the 3D s-SAMO band. Thus, the intermolecular interaction and the dimensionality of the extended bands have a modest effect on reducing the LUMO−SAMO gap.

Fullerene Size Dependence. We have calculated the unoccupied electronic structure for different size fullerenes from C_{20} to C_{130}, as summarized in Figure 6, in order to understand the role of the kinetic and potential energy in defining the SAMO energy. The trend in Figure 6 shows that increasing the cage size increases the s-SAMO binding energy with respect to the vacuum level. The kinetic energy effect counteracts the deeper central potential of smaller fullerenes to destabilize their superatom states.

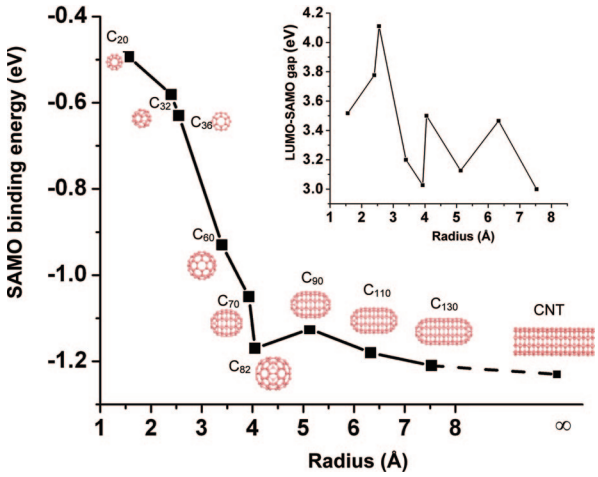

Figure 6. Correlation of the SAMO binding energy with respect to the vacuum level (E_V) and the LUMO (inset) with the size and shape of fullerenes.

When the fullerene size becomes sufficiently large for the central potential to tend to zero, the SAMO binding should approach that of the lowest IP state of a graphene sheet (−1.17 eV).[40] Additional stabilization can be achieved for larger fullerenes (C_{70}, C_{90}, C_{110}, and C_{130}) by keeping the same minor axis while extending the major axis. Increasing the length in one dimension decreases the kinetic energy in that dimension, while keeping the constant core potential, as defined by the minor axis. By extending the axis to infinity, the binding energy approaches −1.23 eV for a (4,4) carbon nanotube.[49]

Because different physical principles determine the SAMO and LUMO energies, the LUMO−SAMO gap has much more erratic dependence on the fullerene size and shape (Figure 6, inset) than the SAMO binding energy. Whereas the core potential depends mainly on the molecular dimensions, the LUMO energy depends on the total number of the valence electrons and the symmetry-dependent orbital degeneracies. The LUMO−SAMO gap, however, never decreases below about 3.0 eV. Therefore, changing the cage size is not very effective in stabilizing the SAMO energy with respect to the LUMO.

Exohedral Doping. A_3C_{60} fullerites, where A stands for the exohedrally doped K, Rb, or Cs, are known superconducting materials.[5] We investigated the SAMO electronic structure of single C_{60} with 1−3 external Li or K atoms. As noted already, alkali atoms, with their low ionization potentials, donate their valence ns electrons to the LUMO of C_{60} molecules, thereby creating a positive ionic potential outside the C atom cage, and moving the Fermi level into the LUMO. Despite experiencing additional stabilizing potential, the lowest s-SAMO band, nevertheless, remains at about 2.8 eV above the LUMO. This result is essentially independent of the alkali atom ionization potential or the number of alkali atoms per C_{60} molecule (we tested A_xC_{60}, where $x = 1$ and 3). The external doping is ineffective in reducing the SAMO energy because C_{60} acts as a Faraday cage;[50,51] the collective response of the 240 valence electrons per C_{60} molecule effectively screens the states that are confined by the cage from the Coulomb potential of an external charge.

We have also investigated 2D aggregates with the Li_2C_{60} stoichiometry. The orbitals of the dopant Li ions hybridize with the π orbitals of C_{60} molecules, giving the hybrid HOMO, LUMO, and LUMO+1 states more dispersive character (Figure 7) as compared with the undoped C_{60} molecule quantum well (Figure 4). This tendency has already been noted for metal atom intercalated C_{60} solids.[52,53] Notwithstanding, the doping with Li atoms hardly affects the s-SAMO band. In the case of the p_z and p_x/p_y orbitals, which have most of their density outside of the cage, the interaction with the ex-

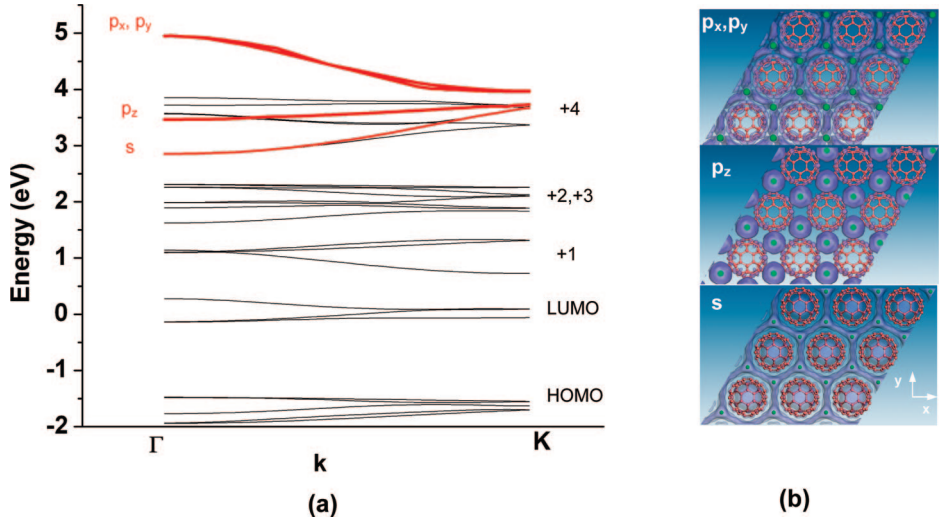

Figure 7. (a) Band structure of a 2D Li_2C_{60} layer (external doping with Li atoms). The red lines show the energy bands formed by the SAMOs. (b) Orbital distributions for s, p_x, p_y, and p_z SAMOs at the Γ point. Li atoms are indicated by the green spheres.

TABLE 4. Electronic Configurations and Ionization Potentials of the Endohedral Atoms and SAMO Energies with the Metal Atom at the Center[a] and at the Most Stable Position[b] (*d* is the distance in nm between the most stable position and the center of C_{60} molecule)

doping atom	electron configuration	ionization potential (eV)	s-LUMO−SAMO gap[a] (eV)	*d* (nm)	s-LUMO−SAMO gap[b] (eV)
Li	[He], $2s^1$	5.40	1.20	0.146	2.05
Na	[Ne], $3s^1$	5.12	1.29	0.080	1.62
K	[Ar], $4s^1$	4.36	2.81	0.013	2.81
Rb	[Kr], $5s^1$	4.18	3.03	0.000	3.03
Cs	[Xe], $6s^1$	3.89	3.38	0.000	3.38
Ca	[Ar], $4s^2$	6.14	0.48	0.115	1.66
Er	[Xe], $4f^{12}6s^2$	6.14	0.15	0.118	1.71
Cu	[Ar], $3d^{10}4s^1$	7.73	−0.52	0.000	−0.52

[a]Doping atom at the center of C_{60}. [b]Doping atom at the optimized position.

ternal Li cations causes their bands to become more localized as evidenced by their larger effective masses and smaller hopping integrals β.

Endohedral Doping. Because screening renders the exohedral doping with alkali atoms as a method for stabilizing the superatom state ineffective, we also investigated the effect of the endohedral doping.[54,55] We performed electronic structure calculations with single alkali, alkaline earth, noble metal, and rare earth metal atoms at their equilibrium position, which is usually off-center near the C atom shell, and in the center of the fullerene cage. First, we illustrate the effect of metal atom doping by the example of endohedral Li atom displaced to the center of C_{60} molecule and also at its most stable site 0.15 nm from the center of C_{60} toward the center of one of its C atom hexagons.

The coincidence of the Li ion and C_{60} molecule potentials within the hollow molecule core causes the atom and superatom electronic states to hybridize. Because of the relatively low ionization potential (see Table 4) of Li and high (~4 eV) electron affinity of C_{60},[56] the 2s electron of Li is completely transferred to its fullerene host. For Li in the center of C_{60} cage, the interaction between the unoccupied 2s orbital of Li and s-SAMO decreases the LUMO−SAMO gap for the hybridized orbital by ~2 eV with respect to the undoped case. Even though they retain some diffuse character, the hybridized orbitals are more localized within the hollow shell than parent SAMOs, as can be seen by comparison of the orbitals in Figures 1a and 8a. The p- and especially d-SAMOs are hardly affected by the endohedral doping because the respective p and d orbit-

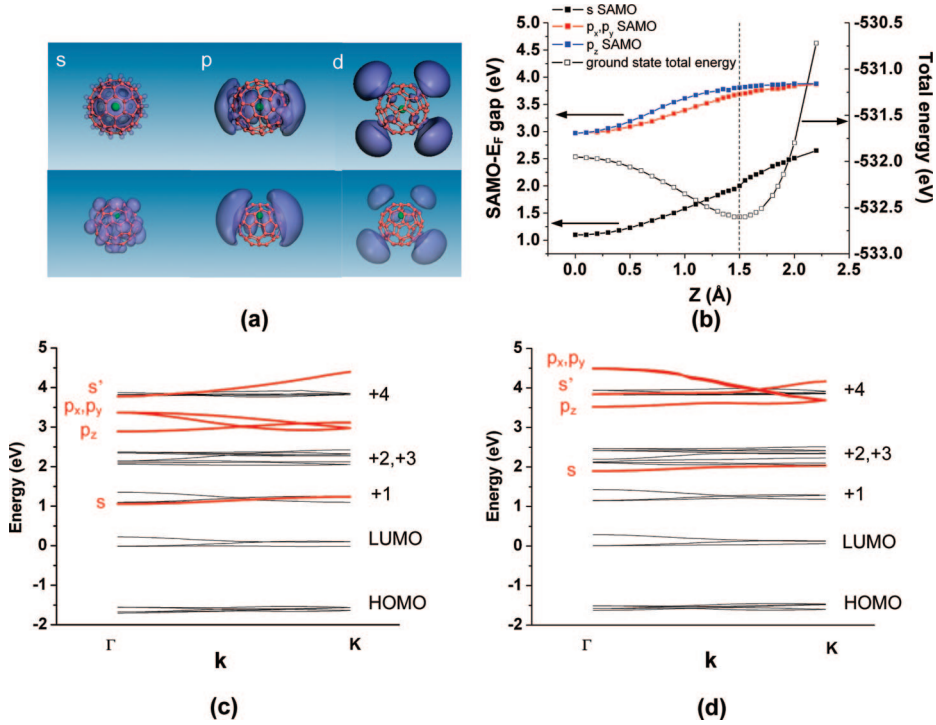

Figure 8. (a) Hybrid SAMO−Li atom orbitals for Li@C_{60} with Li at the center of and at the most stable position within C_{60} molecule. (b) Energy change of SAMOs in Li@C_{60} calculated for the displacement of Li atom from the center of C_{60} molecule through its most stable position (dashed line) at 0.15 nm from the center. The potential surface for the radial displacement of Li atom is also plotted. (c) Band structure of a 2D quantum well of Li@C_{60} with Li at the center, and (d) at its most stable position. The next higher $n = 4$ and $l = 0$ SAMO is indicated by s′.

als of endohedral atoms, with which they can hybridize, are at significantly higher energy than the 2s orbitals.

For a 2D quantum well, with the Li atom in the center of C_{60}, the s-, p_z-, and p_x/p_y-SAMOs are stabilized, respectively, to 1.05, 2.89, and 3.37 eV above E_F at the Γ point (Table 3). The dispersion of the SAMO-derived bands (Figure 8c), however, is weaker than for the undoped C_{60} molecule quantum well (Figure 4a). The m^* of the s-SAMO band, however, at about $2m_e$ is still smaller than for the LUMO. Besides the charge transfer from Li atoms, the endohedral doping has a negligible effect on the LUMO states. Even stronger stabilization of SAMOs can be achieved with higher ionization potential atoms such as Ca (valence of +2), Er (+3), and Cu (+1) (Table 4). Therefore, the strength of the central potential can be tuned primarily by choice of the magnitude of the ionization potential. Other factors, such as the ion size (Pauli exclusion) and the valence of the dopant atom also influence the LUMO−SAMO gap. For the endohedral Ca and Er, the hybrid state can be brought closer to the LUMO than for Li. With even larger ionization potential, the hybrid SAMO for $Cu@C_{60}$ is occupied with a LUMO−SAMO gap of −0.52 eV, as we will discuss in detail. The larger stabilization, however, leads to more localized orbitals that have pronounced endohedral metal atom character.

As already noted, the center of C_{60} molecule is not the equilibrium position for many dopant atoms. Translating the dopant atom from the fullerene center weakens the hybridization of its orbitals with SAMOs, and the symmetry reduction allows many states to interact, causing the hybrid orbitals to acquire more complex shapes that can be seen in Figure 8a. Figure 8b shows the change in energy of the s- and p-SAMO orbitals when Li is displaced from the center through its most stable position 0.15 nm from the C_{60} center. At the equilibrium position of Li, the lowest SAMO energy increases by 0.85 to 2.05 eV above E_F. For the other endohedral fullerenes we have investigated, the displacement of the most stable position from the C_{60} center and the LUMO−SAMO gaps at the center and most stable positions are given in Table 4. As can be seen, the large alkali atoms (K, Rb, and Cs) and Cu occupy the center position. The location of the large alkali atoms is related to their typical chemisorption height on metals, which is comparable with the C_{60} molecule radius.[48] Because the large alkali atoms have small ionization potentials and large excluded volumes, their LUMO−SAMO gaps are comparable to the undoped C_{60} molecule. By contrast, the endohedral Cu stabilizes s-SAMO below the LUMO.

$Cu@C_{60}$, a Molecular Metal? $Cu@C_{60}$ is unique among the s-electron metals that we have studied in its ability to stabilize s-SAMO below LUMO at its equilibrium position within the C atom cage. The two properties are inter-related and can be attributed to the large ionization potential of Cu atoms. As already discussed, low ionization potential metals are ionized and drawn toward the C atom shell by the Coulomb interaction. Higher ionization potential metal atoms, however, by retaining their s-electron experience a repulsive interaction with the C atom shell.

Relevance to Other NFE State of Layered Materials. Our approach to modifying the properties of SAMOs through the endohedral doping has a close correspondence to the intercalation of graphite with metal atoms. When graphene sheets are stacked into graphite, the image potential states of the interacting layers hybridize into the so-called interlayer states, which retain the NFE properties in the interstitial space.[40] The hybridization of the 2D NFE states of graphene with the valence states of the intercalated alkali atoms has been described by theory already in the pioneering work of Posternak and Holzwarth and co-workers.[41,57,58] It has been postulated that superconductivity of intercalated graphite emerges when the hybrid interlayer state becomes partially occupied.[5,24,25,59] The stabilization of interlayer state by Li intercalation has been documented for increasing Li concentration by the inverse photoemission spectroscopy.[59] The Fermi surface for the occupied interlayer state of the superconducting material C_6Ca has been studied by photoemission spectroscopy.[25]

The SAMOs of C_{60} molecules are 0D analogues of the interlayer states formed by wrapping a graphene sheet into a hollow sphere.[17] Like the interlayer states, SAMOs can be stabilized by hybridization with the s-electron states of endohedral metal atoms. On the basis of the analogy with the intercalated graphite compounds and our calculations, we predict that, if they can be synthesized, materials for which the hybrid SAMO−metal atom orbitals are predicted to be partially occupied, such as $Cu@C_{60}$, would have properties of molecular metals. Moreover, because the equilibrium position of a metal atom within the fullerene cage depends on its charge state, we expect that such materials would exhibit strong electron−phonon interaction, which may impart superconducting properties. On the basis of their common physical origins, we propose that tailoring the electronic properties of states derived from the image potential states of graphene, such as the SAMOs of fullerenes, could lead to molecular materials with extraordinary electronic properties.

Moreover, SAMO properties are not only confined to fullerenes. Indeed, 1D NFE states of carbon and BN nanotubes (CNT and BNNT) have already been studied theoretically.[60−63] Because these states are in fact the 1D counterparts of s-SAMO of the C_{60} molecule, we expect that CNT and BNNT should also have higher NFE states with p, d, *etc.* character. NFE states of nanotubes are particularly interesting for applications in electrical transport. It is known that the high-field transport in CNTs is limited by the strong electron−phonon interac-

tion between the optical phonons and π electrons that is characteristic of graphitic materials.[64−66] Because SAMOs have a density minimum at the C atom shell, they should be much more weakly coupled to the nuclear degrees of freedom. To be relevant to transport, however, SAMOs need either to be the lowest unoccupied orbital or to cross the Fermi level. This can be achieved either by lowering the energy of SAMOs employing some of the strategies we have discussed, such as metal atom doping, or by increasing the energy of the π bands. In the case of single-wall CNTs, theory predicts that internal doping with positive charge can stabilize the NFE state by more than 3 eV to below E_F.[60] In the case of BNNT, theory predicts that the lowest energy NFE state is actually at the conduction band minimum because of the weak π orbital delocalization within the hexagonal BN sheets.[26] Likewise, hollow water clusters stabilize solvated electrons through long-range polarization interaction in SAMO-like internal states.[67] Therefore, we expect that in materials with reduced hybridization of the $n = 2$ states, for instance, hydrogenated fullerenes, the more diffuse $n = 3$ states could exist below the π bands and their NFE bands could give rise to novel electronic transport properties.

CONCLUSIONS

In summary, by DFT electronic structure calculations, we have studied the superatom molecular electronic structure of C_{60} and related molecules. The central exchange and correlation potential of hollow molecules gives rise to SAMOs, which are the $n = 3$ solutions of the Schrödinger equation for the combined C atom shell and hollow core potentials. Like the IP states of graphene, which have a similar origin, SAMOs are delocalized over the entire C_{60} molecule. As a consequence of the central core potential, SAMOs have approximate shapes of the s, p, and d orbitals of H or alkali atoms.

To test whether C_{60} molecules and related fullerenes could be used as building blocks of conducting molecular crystals and molecule-based electronic devices, where the atom-like SAMOs could impart novel electron transport properties, we studied the modification of SAMOs through the intermolecular hybridization, cage size, and metal atom doping. When C_{60} molecules are combined into 1D, 2D, and 3D assemblies, SAMOs hybridize into energy bands with strong NFE dispersion. The energies of SAMOs can be tuned most effectively by inclusion of endohedral metal atoms, whereby the hybrid bands may become partially occupied and impart metal-like conductivity to such molecular solids. For most of the systems we have studied, SAMO states are above the LUMO states and, therefore, are unlikely to be relevant for electrical transport. In the case of $Cu@C_{60}$, however, the hybrid state formed by the interaction of the s-SAMO of C_{60} molecule and the 4s state of Cu is partially occupied; within a 2D quantum well of $Cu@C_{60}$, the hybrid state forms a band with an electron mass of $2.8m_e$ midway between the essentially unperturbed HOMO and LUMO orbitals of the parent fullerene. Because the occupation of SAMOs mainly depends on the ionization potential of the endohedral atom, we expect other metals with ionization potentials comparable or larger than copper to stabilize s-SAMO to below the LUMO. Although the 140 meV bandwidth of the conduction band of $Cu@C_{60}$ solid is not large, it should be considered as a lower limit because our DFT-based method does not include the long-range polarization interaction, and therefore, it underestimates the SAMO hybridization.[40]

The paradigm for the intermolecular orbital hybridization and potentially transport exploiting the diffuse nature of the SAMOs is completely different and potentially much more efficient than that derived from the intermolecular hybridization of the more tightly bound and strongly directional σ and π orbitals of aromatic molecules. Therefore, we believe that if materials such as $Cu@C_{60}$ that form partially occupied SAMO-derived bands could be synthesized[68−70] they would find strong interest in molecular electronics, solar energy, correlated materials, *etc.* communities. In conclusion, we have described a novel class of electronic materials and quantum structures that derive their unusual electronic properties from the diffuse $n = 3$ states of hollow molecules.

THEORETICAL FRAMWORK

Because SAMOs are diffuse orbitals, it is impractical to describe them with atomic basis sets. Although the $n = 3$ states with similar character at 2.7 eV above the conduction band minimum have been reported in an early plane-wave basis set calculation for a fullerite solid,[71] SAMOs have escaped scrutiny until their recent experimental observation and characterization by LT-STM.[17] SAMO states also emerge when the band structure theory for solids is adopted to describe the angular momentum properties of a free-electron gas bound to a sphere.[72]

In order to more fully describe the properties of SAMOs by theory, we performed plane-wave basis set DFT electronic structure calculations using the generalized gradient approximation (GGA) with the PBE[73] functional as implemented in the Vienna *ab initio* simulation package (VASP).[74−76] The projector augmented wave (PAW) method was used to describe the electron−ion interaction.[77] The plane-wave basis set cutoff energy was set to 400 eV. For the isolated C_{60} molecule calculation, we used a large cubic unit cell with dimension $a = 3.0$ nm. For the 1D, 2D, and 3D aggregates of C_{60} molecules, we used Monkhorst meshes of ($10 \times 1 \times 1$), ($5 \times 5 \times 1$), and ($5 \times 5 \times 5$), respectively. The distance between the two nearest neighbor C_{60} cores in aggregates was set to 1.0 nm, unless specified otherwise.[18,43] Calculations using the localized density approximation (LDA) produced essentially identical results.

Acknowledgment. We thank A. Rubio, V. Silkin, E. Chulkov, and P. Echenique for discussions of the NFE states of graphene,

and K. D. Jordan for the discussions of the limitations of DFT calculations. We thank the support from grants by the W. M. Keck Foundation, the NSF Grant CHE-0650756, the Petroleum Research Fund (44158-ACS), and Ikerbasque. Calculations were performed in the Environmental Molecular Sciences Laboratory at the Pacific Northwest National Laboratory, a user facility sponsored by the DOE Office of Biological and Environmental Research.

REFERENCES AND NOTES

1. Forro, L.; Mihaly, L. Electronic Properties of Doped Fullerenes. *Rep. Prog. Phys.* **2001**, *64*, 649–699.
2. Guldi, D. M.; Prato, M. Excited-State Properties of C_{60} Fullerene Derivatives. *Acc. Chem. Res.* **2000**, *33*, 695–703.
3. Prato, M. Fullerene Chemistry for Materials Science Applications. *J. Mater. Chem.* **1997**, *7*, 1097–1109.
4. Park, H.; Park, J.; Lim, A. K. L.; Anderson, E. H.; Alivisatos, A. P.; McEuen, P. L. Nanomechanical Oscillations in a Single-C_{60} Transistor. *Nature* **2000**, *407*, 57–60.
5. Gunnarsson, O. Superconductivity in Fullerides. *Rev. Mod. Phys.* **1997**, *69*, 575–606.
6. Wachowiak, A.; Yamachika, R.; Khoo, K. H.; Wang, Y.; Grobis, M.; Lee, D. H.; Louie, S. G.; Crommie, M. F. Visualization of the Molecular Jahn−Teller Effect in an Insulating K_4C_{60} Monolayer. *Science* **2005**, *310*, 468–470.
7. Wang, Y.; Yamachika, R.; Wachowiak, A.; Grobis, M.; Khoo, K. H.; Lee, D. H.; Louie, S. G.; Crommie, M. F. Novel Orientational Ordering and Reentrant Metallicity in K_xC_{60} Monolayers for $3 \leq x \leq 5$. *Phys. Rev. Lett.* **2007**, *99*, 086402.
8. Knupfer, M. Electronic Properties of Carbon Nanostructures. *Surf. Sci. Rep.* **2001**, *42*, 1–74.
9. Hashizume, T.; Motai, K.; Wang, X. D.; Shinohara, H.; Saito, Y.; Maruyama, Y.; Ohno, K.; Kawazoe, Y.; Nishina, Y.; Pickering, H. W.; Kuk, Y.; Sakurai, T. Intramolecular Structures of C_{60} Molecules Adsorbed on the Cu(111)-(1 × 1) Surface. *Phys. Rev. Lett.* **1993**, *71*, 2959–2962.
10. Tsuei, K. D.; Johnson, P. D. Charge Transfer and a New Image State of C_{60} on Cu(111) Surface Studied by Inverse Photoemission. *Solid State Commun.* **1997**, *101*, 337–341.
11. Tsuei, K. D.; Yuh, J. Y.; Tzeng, C. T.; Chu, R. Y.; Chung, S. C.; Tsang, K. L. Photoemission and Photoabsorption Study of C_{60} Adsorption on Cu(111) Surfaces. *Phys. Rev. B* **1997**, *56*, 15412–15420.
12. Wang, L.-L.; Cheng, H.-P. Density Functional Study of the Adsorption of a C_{60} Monolayer on Ag(111) and Au(111) Surfaces. *Phys. Rev. B* **2004**, *69*, 165417.
13. Silien, C.; Pradhan, N. A.; Ho, W.; Thiry, P. A. Influence of Adsorbate−Substrate Interaction on the Local Electronic Structure of C_{60} Studied by Low-Temperature STM. *Phys. Rev. B* **2004**, *69*, 115434.
14. Tautz, F. S. Structure and Bonding of Large Aromatic Molecules on Noble Metal Surfaces: The Example of PTCDA. *Prog. Surf. Sci.* **2007**, *82*, 479–520.
15. Ueno, N.; Kera, S. Electron Spectroscopy of Functional Organic Thin Films: Deep Insights into Valence Electronic Structure in Relation to Charge Transport Property. *Prog. Surf. Sci.* **2008**, *83*, 490–557.
16. Zhu, X. Y.; Dutton, G.; Quinn, D. P.; Lindstrom, C. D.; Schultz, N. E.; Truhlar, D. G. Molecular Quantum Well at the C_{60}/Au(111) Interface. *Phys. Rev. B* **2006**, *74*, 241401.
17. Feng, M.; Zhao, J.; Petek, H. Atomlike, Hollow-Core-Bound Molecular Orbitals of C_{60}. *Science* **2008**, *320*, 359–362.
18. Hou, J. G.; Jinlong, Y.; Haiqian, W.; Qunxiang, L.; Changgan, Z.; Lanfeng, Y.; Bing, W.; Chen, D. M.; Qingshi, Z. Surface Science: Topology of Two-Dimensional C_{60} Domains. *Nature* **2001**, *409*, 304–305.
19. Nakaya, M.; Kuwahara, Y.; Aono, M.; Nakayama, T. Reversibility-Controlled Single Molecular Level Chemical Reaction in a C_{60} Monolayer *via* Ionization Induced by Scanning Transmission Microscopy. *Small* **2008**, *4*, 538–541.
20. Feng, M.; Lee, J.; Zhao, J.; Yates, J. T.; Petek, H. Nanoscale Templating of Close-Packed C_{60} Nanowires. *J. Am. Chem. Soc.* **2007**, *129*, 12394–12395.
21. Because DFT calculations of the molecular HOMO−LUMO gaps are unreliable, we report the calculated SAMO energies with respect to the LUMO. The experimental energies are reported with respect to E_F, which is typically 0.2−0.3 eV below the LUMO for many metals, such as Cu(110) and Cu(111) surfaces.
22. Hybertsen, M. S.; Louie, S. G. Electron Correlation in Semiconductors and Insulators: Band Gaps and Quasiparticle Energies. *Phys. Rev. B* **1986**, *34*, 5390–5413.
23. Lu, X.; Grobis, M.; Khoo, K. H.; Louie, S. G.; Crommie, M. F. Charge Transfer and Screening in Individual C_{60} Molecules on Metal Substrates: A Scanning Tunneling Spectroscopy and Theoretical Study. *Phys. Rev. B* **2004**, *70*, 115418.
24. Csanyi, G.; Littlewood, P. B.; Nevidomskyy, A. H.; Pickard, C. J.; Simons, B. D. The Role of the Interlayer State in the Electronic Structure of Superconducting Graphite Intercalated Compounds. *Nat. Phys.* **2005**, *1*, 42–45.
25. Sugawara, K.; Sato, T.; Takahashi, T. Fermi-Surface-Dependent Superconducting Gap in C_6Ca. *Nat. Phys.* **2009**, *5*, 40–43.
26. Blase, X.; Rubio, A.; Louie, S. G.; Cohen, M. L. Quasiparticle Band Structure of Bulk Hexagonal Boron Nitride and Related Systems. *Phys. Rev. B* **1995**, *51*, 6868–6875.
27. Sakurai, T.; Wang, X. D.; Xue, Q. K.; Hasegawa, Y.; Hashizume, T.; Shinohara, H. Scanning Tunneling Microscopy Study of Fullerenes. *Prog. Surf. Sci.* **1996**, *51*, 263–408.
28. Golden, M. S.; Knupfer, M.; Fink, J.; Armbruster, J. F.; Cummins, T. R.; Romberg, H. A.; Roth, M.; Sing, M.; Schmidt, M.; Sohmen, E. The Electronic-Structure of Fullerenes and Fullerene Compounds from High-Energy Specroscopy. *J. Phys. (Paris)* **1995**, *7*, 8219–8247.
29. Pascual, J. I.; Gomez-Herrero, J.; Rogero, C.; Baro, A. M.; Sanchez-Portal, D.; Artacho, E.; Ordejon, P.; Soler, J. M. Seeing Molecular Orbitals. *Chem. Phys. Lett.* **2000**, *321*, 78–82.
30. Maruyama, Y.; Ohno, K.; Kawazoe, Y. Electronic-Structures of C_{60} and C_{70} Adsorbed on the Cu(111) Surface and Intramolecular STM Images. *Phys. Rev. B* **1995**, *52*, 2070–2075.
31. Weaver, J. H.; Martins, J. L.; Komeda, T.; Chen, Y.; Ohno, T. R.; Kroll, G. H.; Troullier, N.; Haufler, R. E.; Smalley, R. E. Electronic Structure of Solid C_{60}: Experiment and Theory. *Phys. Rev. Lett.* **1991**, *66*, 1741–1744.
32. Saito, S.; Oshiyama, A. Cohesive Mechanism and Energy Bands of Solid C_{60}. *Phys. Rev. Lett.* **1991**, *66*, 2637–2640.
33. Jost, M. B.; Troullier, N.; Poirier, D. M.; Martins, J. L.; Weaver, J. H.; Chibante, L. P. F.; Smalley, R. E. Band Dispersion and Empty Electronic States in Solid C_{60}: Inverse Photoemission and Theory. *Phys. Rev. B* **1991**, *44*, 1966–1969.
34. Gu, B.; Maruyama, Y.; Yu, J.; Ohno, K.; Kawazoe, Y. Effects of Molecular Orientation on the Electronic Structure of Fcc C_{60}. *Phys. Rev. B* **1994**, *49*, 16202–16206.
35. Haddon, R. C.; Brus, L. E.; Raghavachari, K. Electronic Structure and Bonding in Icosahedral C_{60}. *Chem. Phys. Lett.* **1986**, *125*, 459–464.
36. Larsson, J. A.; Elliott, S. D.; Greer, J. C.; Repp, J.; Meyer, G.; Allenspach, R. Orientation of Individual C_{60} Molecules Adsorbed on Cu(111): Low-Temperature Scanning Tunneling Microscopy and Density Functional Calculations. *Phys. Rev. B* **2008**, *77*, 115434.
37. Hou, J. G.; Yang, J.; Wang, H.; Li, Q.; Zeng, C.; Lin, H.; Bing, W.; Chen, D. M.; Zhu, Q. Identifying Molecular Orientation of Individual C_{60} on a Si(111)-(7 × 7) Surface. *Phys. Rev. Lett.* **1999**, *83*, 3001–3004.
38. Lu, X.; Grobis, M.; Khoo, K. H.; Louie, S. G.; Crommie, M. F. Spatially Mapping the Spectral Density of a Single C_{60} Molecule. *Phys. Rev. Lett.* **2003**, *90*, 096802.
39. Dougherty, D. B.; Maksymovych, P.; Lee, J.; Feng, M.; Petek, H.; Yates, J. T., Jr. Tunneling Spectroscopy of Stark-Shifted Image Potential States on Cu and Au Surfaces. *Phys. Rev. B* **2007**, *76*, 125428.
40. Silkin, V. M.; Zhao, J.; Guinea, F.; Chulkov, E. V.; Echenique, P. M.; Petek, H. *Phys. Rev. Lett.* Submitted.

41. Posternak, M.; Baldereschi, A.; Freeman, A. J.; Wimmer, E.; Weinert, M. Prediction of Electronic Interlayer States in Graphite and Reinterpretation of Alkali Bands in Graphite Intercalation Compounds. *Phys. Rev. Lett.* **1983**, *50*, 761–764.
42. Boyle, M.; Hoffmann, K.; Schulz, C. P.; Hertel, I. V.; Levine, R. D.; Campbell, E. E. B. Excitation of Rydberg Series in C_{60}. *Phys. Rev. Lett.* **2001**, *87*, 273401.
43. Nakamura, J.; Nakayama, T.; Watanabe, S.; Aono, M. Structural and Cohesive Properties of a C_{60} Monolayer. *Phys. Rev. Lett.* **2001**, *87*, 048301.
44. Goringe, C. M.; Bowler, D. R.; Hernandez, E. Tight-Binding Modeling of Materials. *Rep. Prog. Phys.* **1997**, *60*, 1447–1512.
45. Campbell, E. E. B.; Hansen, K.; Hoffmann, K.; Korn, G.; Tchaplyguine, M.; Wittmann, M.; Hertel, I. V. From above Threshold Ionization to Statistical Electron Emission: The Laser Pulse-Duration Dependence of C_{60} Photoelectron Spectra. *Phys. Rev. Lett.* **2000**, *84*, 2128–2131.
46. Petek, H.; Ogawa, S. Surface Femtochemistry: Observation and Quantum Control of Frustrated Desorption of Alkali Atoms from Noble Metals. *Annu. Rev. Phys. Chem.* **2002**, *53*, 507–531.
47. Borisov, A. G.; Gauyacq, J. P.; Chulkov, E. V.; Silkin, V. M.; Echenique, P. M. Lifetime of Excited Electronic States at Surfaces: Comparison between the Alkali/Cu(111) Systems. *Phys. Rev. B* **2002**, *65*, 235434.
48. Zhao, J.; Pontius, N.; Winkelmann, A.; Sametoglu, V.; Kubo, A.; Borisov, A. G.; Sanchez-Portal, D.; Silkin, V. M.; Chulkov, E. V.; Echenique, P. M.; Petek, H. Electronic Potential of a Chemisorption Interface. *Phys. Rev. B* **2008**, *78*, 085419.
49. Hu, S.; Zhao, J.; Jin, Y.; Yang, J.; Petek, H.; Hou, J. G. unpublished results.
50. Delaney, P.; Greer, J. C. C_{60} as a Faraday Cage. *Appl. Phys. Lett.* **2004**, *84*, 431–433.
51. Tsukamoto, S.; Nakayama, T.; Aono, M. First-Principles Study on Electronic Responses of a C_{60} Molecule to External Electric Fields. *Chem. Phys.* **2007**, *342*, 135–140.
52. Saito, S.; Oshiyama, A. Ionic Metal K_xC_{60}: Cohesion and Energy Bands. *Phys. Rev. B* **1991**, *44*, 11536–11539.
53. Saito, S.; Oshiyama, A. Sr_6C_{60} and Ba_6C_{60}: Semimetallic Fullerides. *Phys. Rev. Lett.* **1993**, *71*, 121–124.
54. Bethune, D. S.; Johnson, R. D.; Salem, J. R.; deVries, M. S.; Yannoi, C. S. Atoms in Carbon Cages—The Structure and Properties of Endohedral Fullerenes. *Nature* **1993**, *366*, 123–128.
55. Shinohara, H. Endohedral Metallofullerenes. *Rep. Prog. Phys.* **2000**, *63*, 843–892.
56. Ohno, T. R.; Chen, Y.; Harvey, S. E.; Kroll, G. H.; Weaver, J. H.; Haufler, R. E.; Smalley, R. E. C_{60} Bonding and Energy-Level Alignment on Metal and Semiconductor Surfaces. *Phys. Rev. B* **1991**, *44*, 13747–13755.
57. Posternak, M.; Baldereschi, A.; Freeman, A. J.; Wimmer, E. Prediction of Electronic Surface States in Layered Materials: Graphite. *Phys. Rev. Lett.* **1984**, *52*, 863–866.
58. Holzwarth, N. A. W.; Louie, S. G.; Rabii, S. Interlayer States in Graphite and in Alkali-Metal-Graphite Intercalation Compounds. *Phys. Rev. B* **1984**, *30*, 2219–2222.
59. Fauster, T.; Himpsel, F. J.; Fischer, J. E.; Plummer, E. W. Three-Dimensional Energy Band in Graphite and Lithium-Intercalated Graphite. *Phys. Rev. Lett.* **1983**, *51*, 430–433.
60. Miyamoto, Y.; Rubio, A.; Blase, X.; Cohen, M. L.; Louie, S. G. Ionic Cohesion and Electron Doping of Thin Carbon Tubules with Alkali Atoms. *Phys. Rev. Lett.* **1995**, *74*, 2993–2996.
61. Okada, S.; Oshiyama, A.; Saito, S. Nearly Free Electron States in Carbon Nanotube Bundles. *Phys. Rev. B* **2000**, *62*, 7634–7638.
62. Blase, X.; Rubio, A.; Louie, S. G.; Cohen, M. L. Stability and Band Gap Constancy of Boron Nitride Nanotubes. *Europhys. Lett.* **1994**, *28*, 335–340.
63. Blase, X.; Benedict, L. X.; Shirley, E. L.; Louie, S. G. Hybridization Effects and Metallicity in Small Radius Carbon Nanotubes. *Phys. Rev. Lett.* **1994**, *72*, 1878–1881.
64. Yao, Z.; Kane, C. L.; Dekker, C. High-Field Electrical Transport in Single-Wall Carbon Nanotubes. *Phys. Rev. Lett.* **2000**, *84*, 2941–2944.
65. Charlier, J.-C.; Blase, X.; Roche, S. Electronic and Transport Properties of Nanotubes. *Rev. Mod. Phys.* **2007**, *79*, 677–732.
66. Ishioka, K.; Hase, M.; Kitajima, M.; Wirtz, L.; Rubio, A.; Petek, H. Ultrafast Electron−Phonon Decoupling in Graphite. *Phys. Rev. B* **2008**, *77*, 121402.
67. Ogawa, T.; Takagahara, T. Interband Absorption Spectra and Sommerfeld Factors of a One-Dimensional Electron-Hole System. *Phys. Rev. B* **1991**, *43*, 14325–14328.
68. A report of $Cu@C_{60}$ synthesis and characterization by ESR spectroscopy has been published, but this assignment has been questioned and an alternative one to exohedral Cu has been proposed.[69,70]
69. Elliott, B.; Yang, K. Q.; Rao, A. M.; Arman, H. D.; Pennington, W. T.; Echegoyen, L. A Reassignment of the EPR Spectra Previously Attributed to $Cu@C_{60}$. *Chem. Commun.* **2007**, 2083–2085.
70. Huang, H. J.; Ata, M.; Yoshimoto, Y. $Cu@C_{60}$ Formation in Rf-Plasma and Ring-Current Induced Magnetism of C_{60}. *Chem Commun.* **2004**, 1206–1207.
71. Martins, J. L.; Troullier, N.; Weaver, J. H. Analysis of Occupied and Empty Electronic States of C_{60}. *Chem. Phys. Lett.* **1991**, *180*, 457–460.
72. Pavlyukh, Y.; Berakdar, J. Angular Electronic "Band Structure" of Molecules. *Chem. Phys. Lett.* **2009**, *468*, 313–318.
73. Perdew, J. P.; Burke, K.; Ernzerhof, M. Generalized Gradient Approximation Made Simple. *Phys. Rev. Lett.* **1996**, *77*, 3865–3868.
74. Kresse, G.; Hafner, J. *Ab-Initio* Molecular-Dynamics for Open-Shell Transition-Metals. *Phys. Rev. B* **1993**, *48*, 13115–13118.
75. Kresse, G.; Hafner, J. *Ab-Initio* Molecular-Dynamics for Liquid-Metals. *Phys. Rev. B* **1993**, *47*, 558–561.
76. Kresse, G.; Hafner, J. *Ab-Initio* Molecular-Dynamics Simulation of the Liquid-Metal Amorphous-Semiconductor Transition in Germanium. *Phys. Rev. B* **1994**, *49*, 14251–14269.
77. Kresse, G.; Joubert, D. From Ultrasoft Pseudopotentials to the Projector Augmented-Wave Method. *Phys. Rev. B* **1999**, *59*, 1758–1775.